REPURPOSING MU-MIMO DOWNLINK FOR JOINT WIRELESS COMMUNICATIONS AND IMAGING VIA VIRTUAL USERS

Kris Li¹, David Ramirez², Kumar Vijay Mishra³, Ashutosh Sabharwal¹

¹Department of Electrical and Computer Engineering, Rice University, Houston, TX 77005 USA

²DOCOMO Innnovations, Inc., Portland, OR, USA

³United States DEVCOM Army Research Laboratory, Adelphi, MD 20783 USA

ABSTRACT

In this paper, we propose a method to repurpose the multi-user MIMO downlink transmission for joint wireless communication and imaging. The key idea is to introduce the concept of virtual users in the communication coverage area and use the existing MU-MIMO beamforming methods to jointly beamform towards real and virtual users. The virtual users are placed to complement the locations of actual users, with the objective to illuminate the scene as uniformly as possible. We study a single-parameter tradeoff, introduced by a power split parameter between real and virtual users. We demonstrate via simulated examples that the virtual user concept is effective in providing a scalable imaging and communications performance tradeoff for cases where the real users are clustered in small geographical areas.

Index Terms— Communications-centric sensing, Joint sensing and communications, Millimeter wave imaging

1. INTRODUCTION

Joint sensing and communications (JSAC) is emerging as a potential model for next-generation networks [1, 2]. The core idea is to use the transmitted electromagnetic energy for not only communications but also sensing and, more specifically, imaging the physical environment. One class of emerging JSAC system designs is considering the repurposing the communication system designs for both functions [3].

In this paper, we propose a method to leverage the existing multi-user MIMO (MU-MIMO) beamformed network design for joint communications and monostatic imaging. In MU-MIMO systems, e.g., IEEE 802.11n and later standards, the network measures channel response to each real user and then jointly beamforms to the set of communicating users. However, since the users can be located anywhere in the coverage region, the transmitted energy varies for different angles of departure. As a result, the scene is illuminated in a non-uniform manner, leading to a backscattered image reconstruction with gaps where no energy is transmitted. We propose to place virtual users in the spatial gaps and then perform MU-MIMO beamforming to a combination of real and virtual users. By controlling the fraction of power allocated to the virtual users, different rate versus image reconstruction error points can be achieved.

We propose an intuitive heuristic to determine the transmit angles of the virtual data streams based on the distribution of communicating user locations. Finally, we study the system performance via simulations, and quantify the tradeoff between data rates to the real

This work was supported by a grant from Army Research Labs and NSF Grants 1956297, 2215082 and 2148313.

users versus the total image reconstruction error for a scene where real users are clustered along certain angles.

The proposed system is an example of "communicationscentric" design in [3], in that sensing is accomplished utilizing the transmit communication waveform, e.g., MU-MIMO OFDM in a WiFi protocol. Repurposing communication infrastructure for sensing has the potential to expedite the adoption of new network functions by removing the necessity for a dedicated sensing waveform and associated processing chains. Prior work has investigated preamble or probing symbols for opportunistic radar [4, 5]. The use of data symbols for millimeter wave imaging was proposed in [6] using a scanning beam, thereby dedicating the communication system for imaging in certain durations, what can be considered as "imaging-only" modes. In our recent work [7], we proposed the use of MU-MIMO transmissions to real users to opportunistically image using the backscattered communication signals. Since the imaging is opportunistic, the sensing performance is dependent on the location of the real users since the transmit beampatterns are dependent on their measured channel states. Thus if the real users are clustered in a few areas rather than uniformly distributed through the scene, the image reconstruction error can be uneven; we demonstrate with an example in Section 3. Our proposed design develops operating points between opportunistic imaging and imaging-only modes and thus allows a continuous tradeoff between communication and imaging performance measures. We finally note other related work on JSAC waveform design that investigates the radar/comms tradeoff [8, 9]. These works propose solutions to optimization problems that balance radar and communication performance metrics to design an optimized transmit waveform. Our design based on virtual users is comparatively lower complexity since a single parameter controls the sensing gain vs. rate loss. Further, this flexibility is achieved while still utilizing a communication-centric waveform, enabling improved imaging performance even on existing hardware.

2. SYSTEM MODEL

We will adopt the same system model as our recent work [7], which is also summarized in this section. An M-antenna transmit uniform linear array (ULA) is used for MU-MIMO data transmission, while an N-antenna ULA collocated with the transmitter receives the backscattered signal; we assume that the receive array can cancel out direct transmission paths between transmit and receive elements. Figure 1 shows the key elements of the system; the definition of a virtual user will be presented in Section 3.

The transmit access point utilizes an orthogonal frequency-division multiple access (OFDMA) transmission that divides the bandwidth B into $N_{\rm RU}$ resource units (RUs). In frequency, each RU

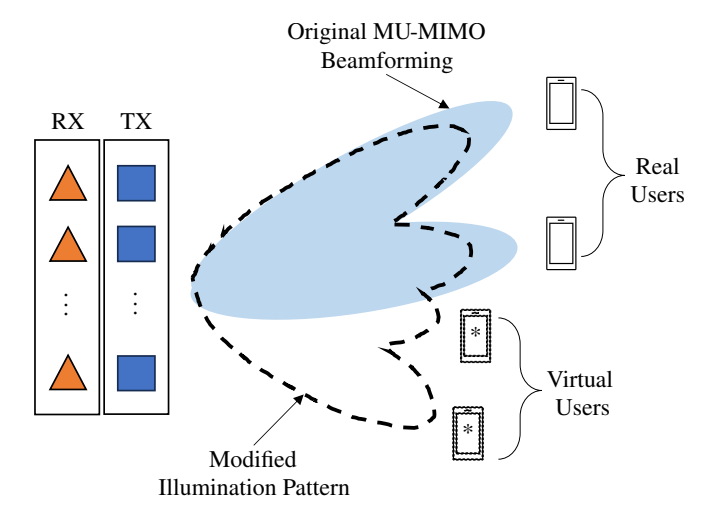


Fig. 1. A collocated MIMO imaging system in which the probing signal is the MU-MIMO downlink data. Adding virtual users allows for new angles to be illuminated and imaged using an existing communication system.

is composed of $K/N_{\rm RU}$ subcarriers, meaning an entire transmitted OFDM symbol consists of K subcarriers. The k-th subcarrier is centered at f_k , $f_k = k\Delta_f$, $k \in [1:K]$, and Δ_f is the subcarrier spacing. In time, we assume the transmission is composed of N_s total OFDM symbols. The transmit antenna array enables spatial multiplexing, and we define U as the number of data streams serviced on the same RU. For a specific OFDM symbol, the $U \times 1$ transmitted user data vector is defined for the k-th subcarrier as $\mathbf{s}_k = \left[s_{1,k}, s_{2,k}, ..., s_{U,k}\right]^T$.

For an M antenna ULA, the $M\times U$ beamforming matrix spatially separates the U users on the same RU:

$$\mathbf{F}_k = \frac{1}{\sqrt{M}} \begin{bmatrix} \mathbf{a}_{\text{TX}}(\theta_{1,k}) & \dots & \mathbf{a}_{\text{TX}}(\theta_{U,k}) \end{bmatrix}$$
(1)

Each column of the precoder $\mathbf{a}_{\mathrm{TX}}(\theta_{u,k})$ is defined as the ULA steering vector towards $\theta_{u,k}$, the angle of the u-th user assigned to the k-th subcarrier. The beamforming codebook $\mathbf{A}_{\Theta,\mathrm{TX}} \in \mathbb{C}^{M \times N_{\Theta}}$ has columns that define $\mathbf{a}_{\mathrm{TX}}(\theta_{u,k})$, with N_{Θ} number of possible transmit angles. Note that while we are defining a beamforming matrix per subcarrier k, in practical systems and in our simulations \mathbf{F}_k varies per RU, i.e. changes every K/N_{RU} subcarriers.

The frequency-domain representation of a single OFDM symbol, indexed at subcarrier k is given as:

$$\mathbf{x}_k = \mathbf{F}_k \sqrt{\mathbf{P}_k} \mathbf{s}_k, \ k \in [1:K] \tag{2}$$

where \mathbf{P}_k is a per-user power allocation matrix and $\operatorname{tr}(\mathbf{P}_k) = P_{\mathsf{TX}}$ such that a per-symbol power constraint of $\frac{P_{\mathsf{TX}}}{M}$ is met, i.e., $\mathbb{E}[\mathbf{x}_k\mathbf{x}_k^H] = \frac{P_{\mathsf{TX}}}{M}\mathbf{I}_M$. Collecting all N_s OFDM symbols, the total transmission is then represented by the matrix $\mathbf{X}_k \in \mathbb{C}^{M \times N_s}$. The $N \times M$ matrix channel is the combined response from L static scatterers located at delay τ_l and angle θ_l :

$$\mathbf{H}(t) = \sum_{l=1}^{L} z_l \delta(t - \tau_l) \cdot \mathbf{a}_{RX}(\theta_l) \mathbf{a}_{TX}^{H}(\theta_l)$$

$$\mathbf{H}_k = \mathcal{F} \{ \mathbf{H}(t) \} \Big|_{f = k\Delta_f}$$
(3)

In the above equation, z_l is the complex reflectivity coefficient that includes path loss and $\mathbf{a}_{\mathrm{RX}}(\theta_l) \in \mathbb{C}^{N\times 1}$, $\mathbf{a}_{\mathrm{TX}}(\theta_l) \in \mathbb{C}^{M\times 1}$ refer to the receive and transmit steering vectors, respectively. Due to the finite aperture size and bandwidth, the scene is quantized into an $N_{\mathcal{R}} \times N_{\Theta}$ grid, where $N_{\mathcal{R}}$ and N_{Θ} are the number of range and angle bins, respectively. We ignore the effect of quantization error on the estimation of the scene, i.e. the scatterers lie perfectly within each grid spot, leading to a $NM \times 1$ vectorized representation of the grid channel response as:

$$\operatorname{vec}(\mathbf{H}_k) = \left([\mathbf{\Psi}_{\mathcal{R}}]_k \mathbf{Z} \mathbf{\Psi}_{\Theta}^T \right)^T \tag{4}$$

where $\Psi_{\mathcal{R}} \in \mathbb{C}^{K \times N_{\mathcal{R}}}$ is the dictionary representing the frequency-response contribution from each range bin, $\Psi_{\Theta} \in \mathbb{C}^{NM \times N_{\Theta}}$ is the dictionary containing the steering vectors towards each angle bin for the NM element virtual array, and $\mathbf{Z} \in \mathbb{C}^{N_{\mathcal{R}} \times N_{\Theta}}$ is the range-azimuth grid. In future simulations, the scene is contained within (20,70) meters and a 120° sector, implying the the range resolution $\delta_{\mathcal{R}} = 50/N_{\mathcal{R}}$ meters and the angular resolution $\delta_{\Theta} = 120^{\circ}/N_{\Theta}$.

The $N \times N_s$ frequency-domain signal matrix at the k-th subcarrier received at the imaging receive ULA is given as:

$$\mathbf{Y}_k = \mathbf{H}_k \mathbf{X}_k + \mathbf{N}_k \tag{5}$$

where N_k is the circularly symmetric Gaussian noise of variance σ_S^2 , leading to the definition of the per-receiver SNR γ_S :

$$\gamma_{\rm S} = \frac{1}{NM} \frac{P_{\rm TX} \left\| \mathbf{H} \right\|_F^2}{\sigma_{\rm s}^2} = \frac{P_r}{N\sigma_{\rm s}^2} \tag{6}$$

Given the receive signal (5) and grid channel representation (4), the imaging receiver performs an image reconstruction to form an estimate of the grid $\hat{\mathbf{Z}}$. We do not detail the exact reconstruction algorithm used in the simulations, although details can be found in our prior work [7]. Instead, this work focuses on the design of the transmit signal to enhance imaging performance. To quantify the quality of the image reconstruction, we introduce the image PSNR, an accepted measure of image quality:

$$PSNR = \frac{\left(\max\{|\mathbf{Z}|\}\right)^2}{MSE(|\mathbf{Z}|, |\hat{\mathbf{Z}}|)} \tag{7}$$

3. VIRTUAL USERS FOR IMAGING

A clear limitation of using backscattered MU-MIMO downlink data to perform imaging is that certain areas of interest may not be illuminated where users are not located. This scenario occurs in realistic network states in which users are spatially clustered rather than being uniformly distributed throughout the scene. To improve the uniformity of the illuminated area, we propose introducing virtual users that are non-interfering with the downlink users. Data streams directed towards the virtual users serve as illumination to image parts of the scene that would otherwise yield gaps in the image reconstruction.

We introduce V virtual users to a given time/frequency resource and define the modified $M \times (U + V)$ precoder \mathbf{F}'_k as:

$$\mathbf{F}_{k}' = \begin{bmatrix} \mathbf{F}_{k} & \mathbf{F}_{k}^{\text{vir}} \end{bmatrix}$$

$$= \begin{bmatrix} \mathbf{F}_{k} & \frac{1}{\sqrt{M}} \mathbf{a}_{\text{TX}}(\theta_{1,k}^{\text{vir}}) & \dots & \frac{1}{\sqrt{M}} \mathbf{a}_{\text{TX}}(\theta_{V,k}^{\text{vir}}) \end{bmatrix},$$
(8)

where $\theta_{v,k}^{\text{vir}}$ is the transmit angle of the v-th virtual user on the k-th subcarrier. Stated in the 802.11ax standards in which MU-MIMO is

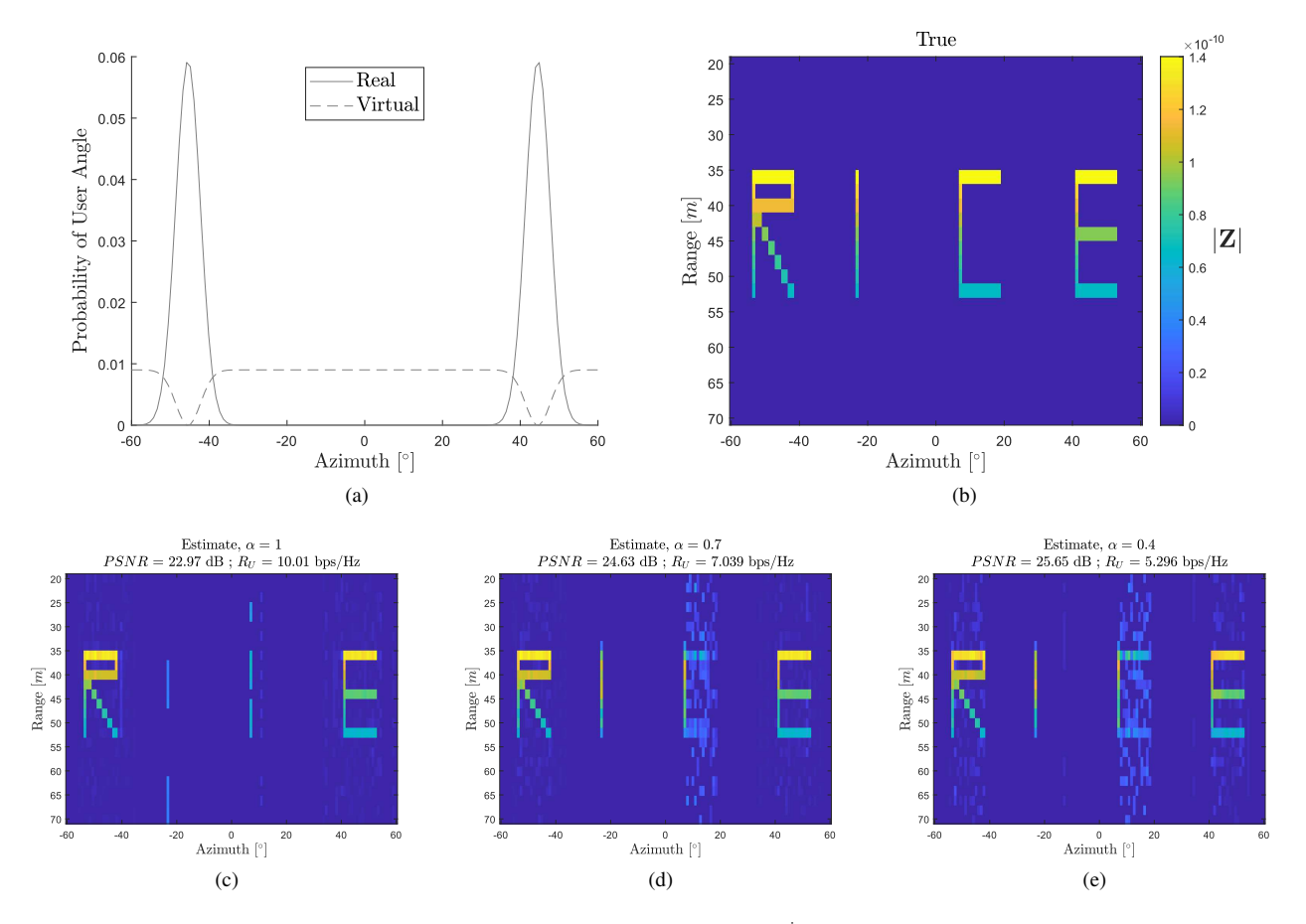


Fig. 2. (a) Example user angle distribution $p(\theta_u)$ and the proposed heuristic for $p(\theta^{\text{vir}})$ in (13); (b) true range-azimuth reflectivity profile; The example images are taken for U=1, V=7: (c) image reconstruction for $\alpha=1$, i.e., no virtual data streams; (d) image reconstruction for $\alpha=.7$; (e) image reconstruction for $\alpha=.4$

supported [10], the maximum number of users supported on a single RU is constrained to no more than 8, so we define U' = U + V and restrict $U' \leq 8$. The symbol vector is modified by appending random data streams to \mathbf{s}_k as $\mathbf{s}_k' = \begin{bmatrix} \mathbf{s}_k & \mathbf{s}_k^{\text{vir}} \end{bmatrix}^T$, and the modified power allocation matrix \mathbf{P}_k' is a $M \times U'$ matrix with the same power budget, $\operatorname{tr}(\mathbf{P}_k') = P_{\text{TX}}$:

$$\mathbf{P}_{k}' = \begin{bmatrix} \alpha \mathbf{P}_{k} & \mathbf{0}_{V} \\ \mathbf{0}_{V} & (1 - \alpha) \mathbf{P}_{k}^{\text{vir}} \end{bmatrix}$$
(9)

Opportunistic imaging, $\alpha=1$: Choosing $\alpha=1$ is akin to opportunistically using the existing communications signal for sensing. In this case, the resulting image quality depends on the spatial distribution of the users.

Balancing Communications with Intentional Imaging, $\alpha \in [0,1)$: Varying the scaling term from $\alpha=1$ to $\alpha=0$ will allocate power towards virtual users, lowering the effective rate of the U real users. When $\mathbf{F}_k^{\text{vir}}$ is designed such that virtual users are angled away from real users, the imaging system coverage and reconstruction quality will be improved. Including the contribution from virtual users to the transmission, the transmit signal can be represented by $\mathbf{X}_k' \in \mathbb{C}^{M \times N_s}$, with each OFDM symbol defined as:

$$\mathbf{x}_{k}' = \mathbf{F}_{k}' \sqrt{\mathbf{P}_{k}'} \mathbf{s}_{k}' \tag{10}$$

The receive signal at the k-th subcarrier follows from modifying the transmit signal in (5) from which $\hat{\mathbf{Z}}$ can be reconstructed.

We assume for simplicity that αP_{TX} is evenly distributed among the U users, and the remaining $(1-\alpha)P_{\mathrm{TX}}$ equally among the V virtual users. Thus, the u-th real user is allocated the power $P_{\mathrm{TX},u}=\alpha\frac{P_{\mathrm{TX}}}{U}$ and the power allocated to the v-th virtual user is given as $P_{\mathrm{TX},v}=(1-\alpha)\frac{P_{\mathrm{TX}}}{V}$. For the real user channels, we only consider a single line-of-sight path along $\theta_{u,k}$, ignoring the effect of the scattering channel. The rate expression in this case is given as:

$$R_{U} = \sum_{u=1}^{U} \log_{2} \left(1 + P_{\text{TX},u} \frac{\left\| \mathbf{h}_{u}^{C} \right\|^{2}}{\sigma^{2} + \sigma_{I,u}^{2}} \right)$$
(11)

where \mathbf{h}_u^C is the channel gain, σ^2 is the noise variance, and $\sigma_{I,u}^2$ is the interference power at the u-th real user:

$$\sigma_{I,u}^{2} = \left\| \mathbf{h}_{u}^{C} \right\|^{2} \left(\sum_{i=1,i\neq u}^{U} P_{\mathsf{TX},u} |\mathbf{f}_{u,k}^{H} \mathbf{f}_{i,k}|^{2} + \sum_{v=1}^{V} P_{\mathsf{TX},v} |\mathbf{f}_{u,k}^{H} \mathbf{f}_{v,k}^{\mathsf{vir}}|^{2} \right)$$

$$(12)$$

The first term in (12) describes the interference power between the u-th user and the U-1 other real users, where $\mathbf{f}_{i,k}$ is the beamforming

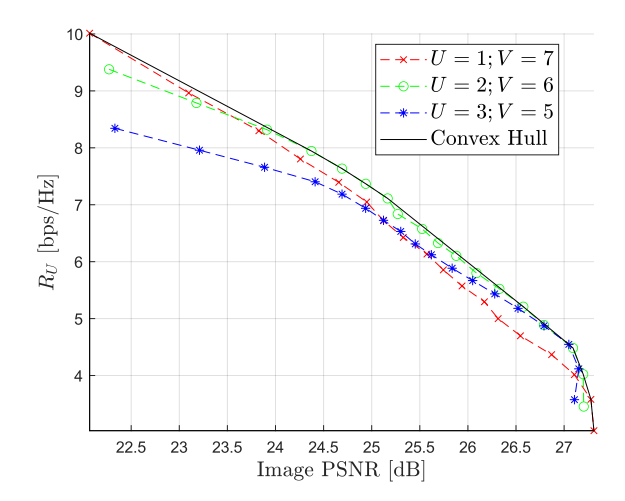


Fig. 3. Tradeoff curves between effective sum spectral efficiency (11) and image PSNR (7) for some pairs (U,V). The user angle distribution and scene are fixed to those in Fig. 2(a) and Fig. 2(b), respectively. The solid line is the convex hull of the tradeoff curves for all (U,V) pairs such that U'=8.

vector associated with the i-th real user. The second term describes the interference between the u-th user and the V virtual data streams, with $\mathbf{f}_{v,k}^{\mathrm{vir}}$ being the steering vector associated with the v-th virtual user

We assume that the real user angles $\theta_{u,k}$ that define \mathbf{F}_k are drawn from a known distribution $p(\theta_u)$. We propose the following heuristic to define the angles of the virtual user data streams:

$$p(\theta^{\text{vir}}) = \frac{\max\{p(\theta_u)\} - p(\theta_u)}{\sum\limits_{\Theta} \left(\max\{p(\theta_u)\} - p(\theta_u)\right)}$$
(13)

This choice of $p(\theta^{\rm vir})$ intends to limit the probability that a virtual data stream is transmitted towards a communicating user, having two related effects: The probability that a virtual data stream strongly interferes with a communicating user is reduced, and the spatial diversity of the transmit signal is improved to enable higher resolution imaging. An example of $p(\theta_u)$ and the resulting distribution for $p(\theta^{\rm vir})$ is given in Figure 2(a). When $\alpha=1$ only the objects along the transmit angles of the real users can be imaged. An example reconstruction for this scenario is given in Figure 2(c), clearly showing that objects at angles where $p(\theta_u)=0$ are lost in the reconstruction. By allocating increasingly more power towards virtual users located at angles drawn from $p(\theta^{\rm vir})$, these objects can be reconstructed due to more spatially diverse illumination as shown in Figures 2(d)-(e).

4. NUMERICAL RESULTS

To demonstrate that the system can flexibly span the imaging and communications tradeoff space, the proposed system is implemented in simulation with the system parameters listed in Table 1. The distributions $p(\theta_u)$ and $p(\theta^{\rm vir})$ in the experiments are drawn in Figure 2(a). Each point along the curves is an average of 1E3 simulation iterations, wherein each has a uniquely generated observation of user positions.

Parameter	Value
f_c	28 GHz
$N_{ m RU}$	60 resource units
K	720 subcarriers
Δ_f	120 KHz
B	86.4 MHz
N_s	14 OFDM symbols
σ^2	10^{-6}
\mathbf{s}_k	16-QAM modulation
N, M	16 antennas
P_{TX}	20 dBm
γ_S	20 dB
$\left\ \mathbf{h}_{u}^{C}\right\ ^{2}$	0 dB
Δ_{TX}, Δ_{RX}	$\frac{1}{2}, M \cdot \frac{1}{2}$
z_l	0 dB
$N_{\mathcal{R}}$	25 range bins
N_{Θ}	128 azimuth bins
L	133 scatterers

Table 1. Constant system parameters

Fixing the scene to that of Figure 2(b), the experimental rate-PSNR tradeoff curves for different choices of U and V, are shown in Fig. 3. Each point along a curve corresponds to reducing α by .05. At $\alpha \approx 1$, lower values of effective rate R_U are observed for higher choice of U due to the high interference power associated with analog beamforming. However, the interference decreases for lower α , and multiplexing gains are observed for the multiuser case. Allocating power towards virtual users leads to improved image reconstruction, demonstrating the system's ability to flexibly tradeoff rate for PSNR. Another similar simulation was performed, but rather than fixing the scene to be the range-azimuth profile given in Figure 2(b), the scatterers were instead uniformly distributed throughout the scene. The trends revealed by the previous simulation hold in this case with minor variation in the exact PSNR values observed, thus we omit the resulting tradeoff curve.

The convex hull of the curves observed for all pairs of (U,V) where $U' \leq 8$ borders the achievable rate-PSNR region of the proposed system for a given $p(\theta_u)$ and scene. The points that make up the convex hull represent the transmit signal parameters (U,V,α) that optimize the imaging quality for a given rate. This characterization of the achievable tradeoff space is particularly useful for a communication-centric sensing waveform design in which a quality-of-service or minimum rate constraint is often considered.

5. CONCLUSION AND FUTURE DIRECTIONS

This work proposed a method to repurpose the MU-MIMO downlink signal for joint wireless communication and imaging. Through the introduction of virtual users, the transmission is modified to improve the spatial diversity and enable higher quality image reconstructions. The system can flexibly span the rate-PSNR tradeoff space by tuning a single parameter that controls the power allocation between virtual and real users. The tradeoff curves for various choices of U and V are measured in simulation, and the convex hull is taken to characterize the achievable rate-PSNR region of the system for a fixed scene and user distribution. The proposed system could enable the expedited deployment of JSAC, given that the virtual user concept can be readily implemented onto current transmit hardware already supporting MU-MIMO.

6. REFERENCES

- [1] F. Liu, Y. Cui, C. Masouros, J. Xu, T. X. Han, Y. C. Eldar, and S. Buzzi, "Integrated sensing and communications: Toward dual-functional wireless networks for 6G and beyond," *IEEE Journal on Selected Areas in Communications*, vol. 40, no. 6, pp. 1728–1767, 2022.
- [2] W. Zhou, R. Zhang, G. Chen, and W. Wu, "Integrated sensing and communication waveform design: A survey," *IEEE Open Journal of the Communications Society*, vol. 3, pp. 1930–1949, 2022.
- [3] J. A. Zhang, F. Liu, C. Masouros, R. W. Heath, Z. Feng, L. Zheng, and A. Petropulu, "An overview of signal processing techniques for joint communication and radar sensing," *IEEE Journal of Selected Topics in Signal Processing*, vol. 15, no. 6, pp. 1295–1315, 2021.
- [4] P. Kumari, J. Choi, N. González-Prelcic, and R. W. Heath, "IEEE 802.11ad-based radar: An approach to joint vehicular communication-radar system," *IEEE Transactions on Vehicular Technology*, vol. 67, no. 4, pp. 3012–3027, 2018.
- [5] E. Grossi, M. Lops, L. Venturino, and A. Zappone, "Opportunistic radar in IEEE 802.11ad networks," *IEEE Transactions on Signal Processing*, vol. 66, no. 9, pp. 2441–2454, 2018.

- [6] J. Guan, A. Paidimarri, A. Valdes-Garcia, and B. Sadhu, "3-d imaging using millimeter-wave 5g signal reflections," *IEEE Transactions on Microwave Theory and Techniques*, vol. 69, no. 6, pp. 2936–2948, 2021.
- [7] K. Li, K. V. Mishra, and A. Sabharwal, "Opportunistic time-of-flight imaging with MU-MIMO downlink," in *Asilomar Conference on Signals, Systems, and Computers*, 2023, in press.
- [8] M. Temiz, E. Alsusa, and M. W. Baidas, "Optimized precoders for massive MIMO OFDM dual radar-communication systems," *IEEE Transactions on Communications*, vol. 69, no. 7, pp. 4781–4794, 2021.
- [9] F. Liu, L. Zhou, C. Masouros, A. Li, W. Luo, and A. Petropulu, "Toward dual-functional radar-communication systems: Optimal waveform design," *IEEE Transactions on Signal Processing*, vol. 66, no. 16, pp. 4264–4279, 2018.
- [10] IEEE Standard for Information Technology— Telecommunications and Information Exchange between Systems Local and Metropolitan Area Networks—Specific Requirements Part II: Wireless LAN Medium Access Control (MAC) and Physical Layer (PHY) Specifications Amendment 1: Enhancements for High-Efficiency WLAN, Std., 2021.